

New phosphorylation route of a series of 2-AlkylBenzimidazole derivatives: Synthesis, characterization, biological evaluation, ADMET prediction, molecular docking and DFT studies

Fatima Youssoufi^{a*}, Manal Zefzoufi^b, Soukaina Elorchi^c, Abouelhaoul El Alami^a, Assiya Atif^a, Abdoul-Hakim Mohamed^c, Mohammed Salah^c, Rabiaa Fdil^a, Mustapha Soufyane^a and Hamid Sdassi^a

^aBioorganic Chemistry Team, Faculty of Sciences, Chouaib Doukkali University, P.O. Box 20, El Jadida, 24000, Morocco

^bSustainable Development and Health Research Team, Faculty of Sciences and Techniques, Cadi Ayyad University, P.O. Box: 549, Marrakech, 40000, Morocco

^cMolecular Modelling and Spectroscopy Research Team, Faculty of Sciences, Chouaib Doukkali University, P.O. Box 20, El Jadida, 24000, Morocco

CHRONICLE

Article history:

Received October 3, 2024

Received in revised form

November 2, 2024

Accepted February 7, 2025

Available online

February 7, 2025

Keywords:

Benzimidazole

Phosphorylation

Antimicrobial activity

ADMET

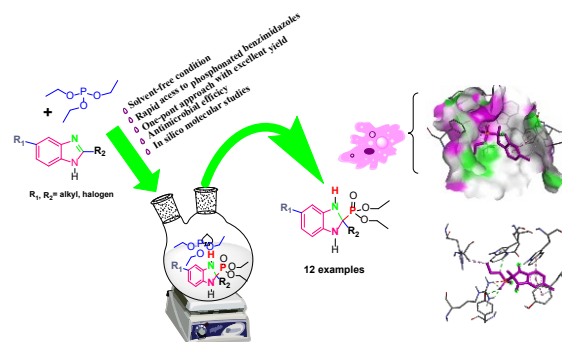
Molecular docking

DFT analysis

ABSTRACT

A series of new benzimidazole phosphonate derivatives was obtained via nucleophilic addition of triethyl phosphite to the imine of the imidazole subgroup under solvent-free conditions. Structures of the formed products were confirmed using spectroscopic data (ATR-FTIR, ¹H-NMR, ¹³C-NMR, and MS). The antimicrobial profiles of the synthesized compounds were examined, and promising activities against *Staphylococcus aureus*, *Escherichia coli*, *Pseudomonas aeruginosa*, and *Candida albicans* were revealed, showing significant inhibition zone diameters ranging from 13 to 17 mm. Alongside these experimental findings, *in silico* investigations were conducted using ADMET characteristics, which showed a positive pharmacokinetic profile and provided valuable information on potential interactions with target molecules. Besides, docking studies against tested microorganisms revealed further insights on the compounds' binding interactions with the active sites. Finally, DFT analysis was performed to shed light on the synthesis of novel molecules.

© 2025 by the authors; licensee Growing Science, Canada.



9

Graphical Abstract

1. Introduction

Heterocyclic nitrogen compounds are being studied by numerous bioorganic research teams as they are scaffolds considerably prevalent in various fields, especially the pharmaceutical industry.^{1–4} On the whole, benzimidazole is an awfully versatile heterocycle and a crucial precursor for the design of biologically active organic compounds. Hence, it is

* Corresponding author

E-mail address fyousoufi04@gmail.com (F. Youssoufi)

well known that the diverse applications of benzimidazole derivatives have been and are still under concentrated investigations due to their intensive uses as antimicrobial (antibacterial, antifungal, antihelminthic/antiparasitic, antiprotozoal, etc.),⁵⁻⁸ antiviral (anti-HIV, anti-HBV and HCV (hepatitis B and C), etc.),^{9,10} anti-inflammatory/analgesic,¹¹ anti-allergic,¹² anti-tuberculosis,¹³ antidepressant,¹⁴ antihypertensive,¹⁵ antioxidant¹⁶ and antitumor/anticancer drugs.^{17,18}

On the other hand, the development of new organophosphorus compounds is increasingly gaining interest, due to the wide spectrum of biological properties possessed by these products.¹⁹ Thus, the introduction of a phosphonate group into a heterocyclic molecule can both synergistically enhance existing useful properties and expand their practical scope of application. Many benzimidazole phosphonates compounds, including nucleotide analogues, have been reported in the literature as drugs used in the treatment of several disorders.^{20,21,22} Among them, fluorinated benzimidazole phosphonates have shown good biological activity towards AMP protein kinase, useful for diabetes prevention (**A**) (Fig. 1).²³ Furthermore, benzimidazole phosphonates derivatives are used as ligands because of their bioactive properties, as well as for the synthesis of microbiologically active complexes with structurally similar ligands. For example, the copper (II) complex of the 1*H*-benzimidazol-2-ylmethyl diethyl phosphate ligand (2-BimOpe (**B**)) was found to be a cytotoxic agent against A549 lung cancer cell lines and a human colorectal adenocarcinoma cell line (HT29) (Fig. 1).²⁰ Additionally, the silver (I) complex of 1*H*-benzimidazol-2-ylmethyl diethyl phosphate [Ag(2-bimOpe)₂]₂NO₃ (**C**) is a compound particularly active against *Pseudomonas aeruginosa* and methicillin-resistant *Staphylococcus epidermidis* (Fig. 1).²⁴

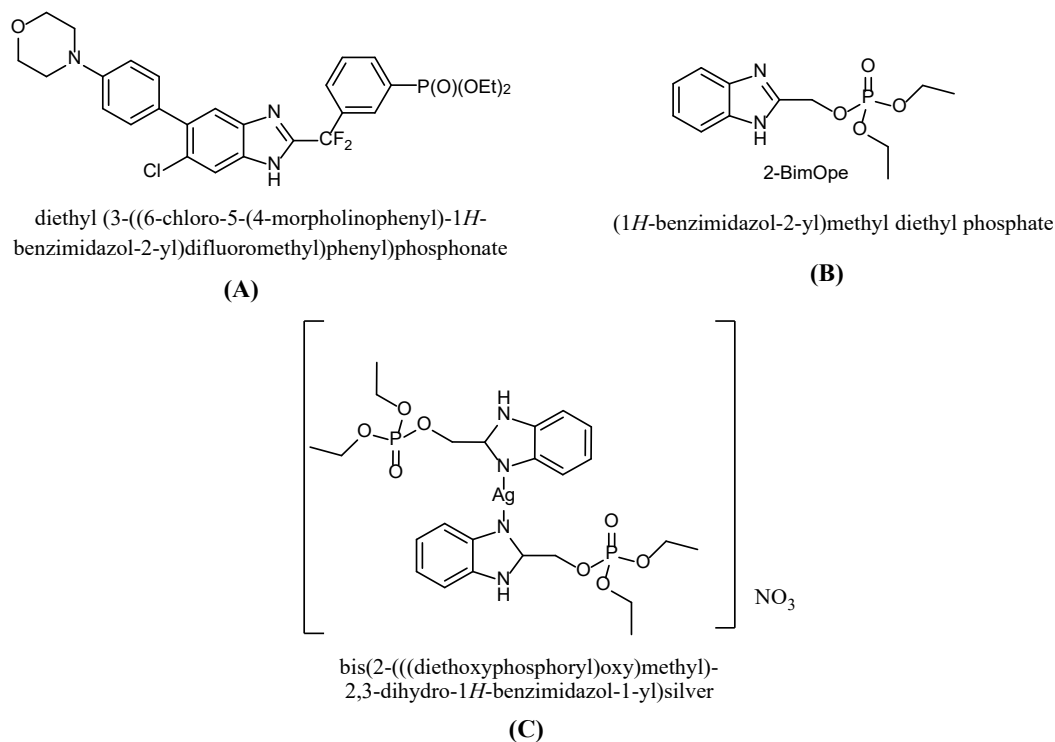


Fig. 1. Chemical structures of medicinal benzimidazole phosphonates

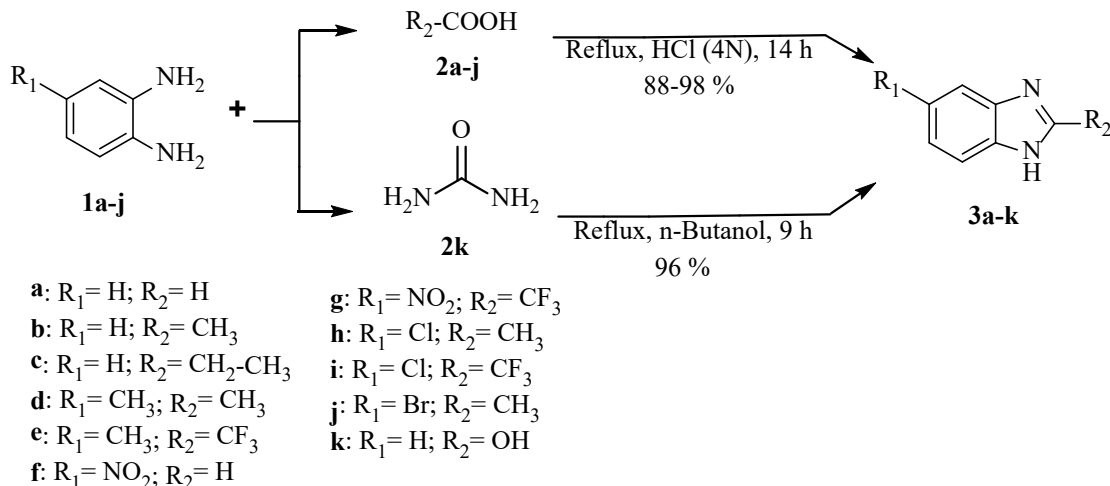
The formerly mentioned biological as well as biochemical relevance of benzimidazole derivatives and phosphonates prompted us to develop a new synthetic route of new benzimidazole phosphonates through the action of triethyl phosphite on the C=N double bond of 2-alkylbenzimidazole derivatives to build a phosphonate P-C-N system based on works previously published.²⁵ Indeed, the synthesis of cyclic α -substituted- α -aminophosphonates by addition of a phosphonate group onto the imine function of 2-alkylbenzimidazole is a novel approach. To this end, a series of α -aminophosphonate compounds, namely (**5a-k**), were synthesized, characterized, and screened *in vitro* for their potential biological activities against three types of microorganisms: two Gram-positive bacteria: *Staphylococcus aureus* and *Pseudomonas aeruginosa*, a Gram-negative bacteria: *Escherichia coli* and *Candida albicans* as fungi. Subsequently, a theoretical study of the synthesized adducts was also conducted using molecular docking, ADMET predictions, and DFT analysis, to allow further exploration and forecasting of the compounds' bioactivity. Hence, coupling experimental and computational studies improves our understanding of these chemicals' interactions with target molecules (proteins), in order to assess their biological potency and broad their application areas.

2. Results and Discussion

2.1 Chemistry

2.1.1 Synthesis of benzimidazole derivatives (3a-k)

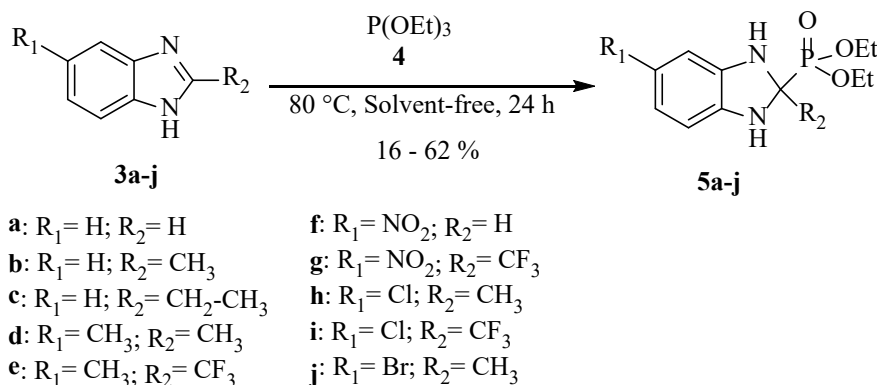
2-alkylbenzimidazoles (**3a-j**), used in the phosphorylation reaction, were synthesized according to the procedure described by Phillips (Scheme 1).²⁶ This reaction involves the condensation of 1,2-phenylenediamine derivatives **1a-j** with carboxylic acids **2**. Compounds **3a-j** were obtained in good yields (88-98 %). Besides, compound **3k** was synthesized from 1,2-phenylenediamine and urea in refluxing n-butanol to isolate 2-hydroxybenzimidazole **3k** (Scheme 1).²⁷



Scheme 1. Synthesis of benzimidazole derivatives (**3a-k**)

2.1.2 Phosphorylation of benzimidazoles (3a-k)

Phosphorylation of benzimidazole derivatives has been described in the literature according to various methods.^{28,29} In this work, we present a new synthetic route of benzimidazole phosphonates using 2-alkylbenzimidazole derivatives **3a-k** and triethyl phosphite **4** as starting precursors, under solvent-free conditions and in the absence of the catalyst at 70-120 °C for 24-72 h (**Scheme 2**). The best results were obtained at 80 °C and for 24 h as the optimized reaction conditions. A simple nucleophilic addition of the phosphorous group on the cyclic imine of benzimidazole characterizes this approach. The target compounds **5a-k** were obtained with oily and solid aspects in moderate to good yields (15-62 %). All synthesized products were characterized by IR spectroscopy, (¹H, ¹³C) NMR, and mass spectrometry spectral data.

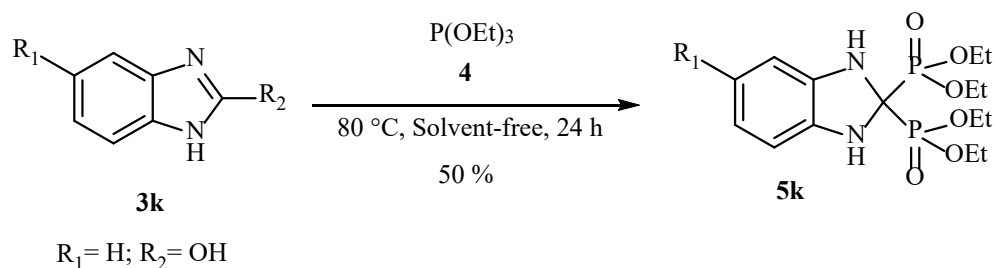


Scheme 2. Phosphorylation of benzimidazole derivatives (**3a-j**)

The IR spectrum of isolated compound **5a** shows the appearance of an absorption band at 1276 cm⁻¹ corresponding to the stretching of the P=O group confirming the addition of triethyl phosphite on the C=N band of the cyclic imine. In addition, the spectrum also reveals the presence of absorption bands at 1227 and 3373 cm⁻¹ attributed to imidazole CH and NH groups, respectively. Besides, the ¹H-NMR spectrum of diethyl (2,3-dihydro-1H-benzimidazol-2-yl) phosphonate **5a** reveals the presence of a triplet at 1.36 ppm corresponding to the six protons of the methyl phosphate groups -P-(O-CH₂-CH₃)₂, a quadruplet signal was also recorded at 4.23 ppm attributed to the four protons of the two methylene groups -P-(O-CH₂-CH₃)₂, and a double signal resonates at 7.20 ppm attributed to the proton (CH) of the imidazole ring. Chemical shifts of the aromatic protons were detected in the range 7.57-7.63 ppm, and finally, the chemical shift of the two amine protons (-NH) of the imidazole ring was recorded as a singlet at 8.27 ppm. On the other hand, the ¹³C-NMR spectrum shows, in particular, that the carbon atom belonging to the -CH group of imidazole presents a double signal at 59.6 ppm attributed to

the presence of the phosphorus nucleus. Moreover, two signals were recorded at 16.4 ppm and 16.5 ppm and were assigned to the two carbons of the two CH₃ groups. In addition, the spectrum reveals the presence of two other signals at 63.6 ppm and 63.6 ppm assigned to the two carbons of the methylene group (CH₂) linked to phosphorus. Furthermore, signals recorded at 110.9, 119.7, 122.1, 122.8, 133.9 and 143.4 ppm are attributed to the aromatic ring carbons. The characteristic NMR signals of the synthesized compounds were consistent with those of similar compounds previously reported.^{30,31} Finally, the mass spectrum of compound **5a** shows the presence of a molecular peak at $m/z = 256$ [M]⁺ confirming the proposed structure.

Furthermore, phosphorylation of 2-hydroxybenzimidazole **3k** was carried out using the same procedure previously described, yielding a bisphosphonate compound (tetraethyl (2,3-dihydro-1*H*-benzimidazol-2,2-diyl)bisphosphonate) (**Scheme 3**). The structure of benzimidazole bisphosphonate **5k** was established by IR, (¹H, ¹³C) NMR, and mass spectral data.



Scheme 3. Phosphonylation of 2-hydroxybenzimidazole **3k**

2.2 Biological Screening

2.2.1 Antimicrobial Activity

Benzimidazoles phosphonates **5a-j** were tested, *in vitro*, for their antibacterial and antifungal activities against tree human pathogenic bacteria; *E. coli*, *S. aureus*, *P. aeruginosa*, and *C. albicans* as fungi. For that, the antimicrobial activity was evaluated using the agar disc diffusion technique to measure the inhibition diameter. The formation of inhibition zones around the wells demonstrates microbial sensitivity to compounds. The obtained results are summarized in table 1. Compared with the standard compounds, these products generally exhibited moderate to excellent effectiveness in antibacterial and antifungal activities. Among the active products, compound *diethyl (5-chloro-2-methyl-2,3-dihydro-1*H*-benzimidazol-2-yl)phosphonates (5h)* showed higher antibacterial activity against *E. coli*, *S. aureus* and *P. aeruginosa* at 500 ppm with inhibition zones of 15 mm, 16 mm, and 15 mm, respectively. This result was achieved thanks to the presence of a chlorine atom in the compound's structure, making it highly effective at inhibiting bacterial growth. The next active compound was *diethyl (2-methyl-2,3-dihydro-1*H*-benzimidazol-2-yl)phosphonate (5b)* which also displayed a significant inhibition activity with inhibition zones of 15 mm, 16 mm, and 14 mm, respectively, compared with the standard drug (*Ciprofloxacin*; 19 mm, 20 mm, and 22 mm, respectively). As can be seen in Table 1, it is clear that the effectiveness of **5b** and **5h** against *S. aureus* was more than other compounds. Besides, compounds **5g** and **5i** showed good activity against *P. aeruginosa*, whereas they displayed an important antibacterial activity against *E. coli* and *S. aureus*. This can be explained by the presence of a trifluoromethylated group in the structure of their molecules, giving them a longer lifespan and enabling them to resist diverse pathogenic bacteria. With regard to antifungal results, we observed that two compounds (**5b** and **5h**) have higher anticandidal activity against *Candida albicans* with an inhibition zone of 17 mm compared with the standard drug (*Fluconazole*; 18 mm), followed by compound **5i** (15 mm), compound **5c** (14 mm), and compound **5g** (13 mm). Therefore, these promising results enable these compounds to play a significant role in the development of new antifungal agents, particularly in view of the limited number of antifungal drugs currently available for the treatment of invasive fungal infections caused by the emergence of additional drug-resistant species, such as *Candida*.³² However, no antimicrobial effect was exhibited by the compounds **5a**, **5d**, **5e**, **5f** and **5j**. Although these compounds are inactive against tested drugs, they are suitable lead compounds for the generation of more active analogs in the future.

In order to evaluate the Minimum Inhibitory Concentration (MIC) of the synthesized compounds against pathogenic bacteria and fungi, a broth microdilution experiment was used as reported by Anthony et al..³³ Table 2 presents different MIC values of the obtained products. Compounds **5b**, **5h**, and **5i** exhibited the best antimicrobial activity against all bacterial and fungal strains with the lowest MIC values. Indeed, compounds **5b** and **5h** showed higher antifungal activity against *C. albicans* with an MIC of 31.25 ppm, whereas compound **5i** showed an important activity against *C. albicans* with an MIC = 62.5 ppm. On the other hand, compound **5h** displayed excellent antibacterial activity against *E. coli* and *S. aureus* with an MIC = 62.5 ppm. The antimicrobial action of some compounds may be due to their potential ability to adhere to the cell membrane surface, interfering with cell permeability and respiration processes. In fact, the backbone structure of any compound plays an essential role in biological assessments; moreover, it is possible that the efficacy of compounds enables them to penetrate more easily and support a broad surface area for greater interaction with microorganisms, promoting powerful antimicrobial activity. To our knowledge, this is the first time that the synthesized compounds have demonstrated antimicrobial action. These findings are in line with previous research on the antimicrobial action of benzimidazole phosphonates, and underline the prospective use of these products to inhibit harmful microorganisms.²⁴

Table 1. Inhibition zones of compounds (**5b**, **5c**, **5g**, **5h** and **5i**) and controls (Ciprofloxacin and Fluconazole) against three pathogenic bacteria and one fungi

Compound	Inhibitory zones diameter (mm)			
	Bacteria			Fungi
	<i>E. coli</i>	<i>S. aureus</i>	<i>P. aeruginosa</i>	<i>C. albicans</i>
5b	15 ± 0.02	16 ± 0.11	14 ± 0.2	17 ± 0.15
5c	NE	NE	NE	14 ± 0.01
5g	14 ± 0.12	14 ± 0.25	13 ± 0.05	13 ± 0.05
5h	15 ± 0.12	16 ± 0.25	15 ± 0.05	17 ± 0.05
5i	14 ± 0.12	13 ± 0.25	13 ± 0.05	15 ± 0.05
Fluconazole	-	-	-	18 ± 0.02
Ciprofloxacin	19 ± 0.1	20 ± 0.1	22 ± 0.1	-
DMSO	/	/	/	/

/: Inactive; NE: No Effect; ±: standard deviation.

Table 2. Minimum Inhibitory Concentration (MIC) (ppm) of compounds **5b**, **5c**, **5g**, **5h**, and **5i** on three pathogenic bacteria and one fungi

Compound	Minimal Inhibitory Concentration (MIC) (ppm) ^{a)}			
	Bacteria			Fungi
	<i>E. coli</i>	<i>S. aureus</i>	<i>P. aeruginosa</i>	<i>C. albicans</i>
5b	150 ± 0.1	125 ± 0.2	175 ± 0.11	31.25 ± 0.1
5c	NE	NE	NE	150 ± 0.2
5g	125 ± 0.11	125 ± 0.2	275 ± 0.15	175 ± 0.12
5h	62.5 ± 0.1	62.5 ± 0.15	250 ± 0.15	31.25 ± 0.05
5i	175 ± 0.12	250 ± 0.25	275 ± 0.22	62.5 ± 0.1

/: Inactive; NE: No Effect; ±: standard deviation.

^{a)} DMSO was introduced to several organisms as a control and revealed no inhibitory zone.

2.3 Computational Studies

In drug discovery, the choice of a candidate demands a vital pharmacokinetic profile, which provides a comprehensive view of the creation of a substantial medicinal product. The results of the biological tests showed that compounds **5b**, **5c**, **5g**, **5h**, and **5i** have significant antimicrobial activity. Hence, to support and confirm these findings, as well as to highlight the search for effective drugs, *in silico* computational studies of the compounds were examined, i.e., ADMET prediction, molecular docking, DFT calculations, and MESP analysis.

2.3.1 In Silico ADMET Properties

Lipinski's rule of five was used to assess the active products' potential as drugs and to predict their oral bioavailability. This rule states that for a molecule to be considered a good candidate for an oral drug, it should not violate more than one of these rules: i) a molecular weight less than 500 Da; ii) a partition coefficient (Log P) less than 5; iii) no more than five hydrogen bond donors; and iv) no more than ten hydrogen bond acceptors.³⁴ The obtained results are presented in **Table 3** and they show that all the achieved compounds do not violate Lipinski's rules, thus explaining their potential antimicrobial activity.

Table 3. Pharmacokinetic parameters of compounds **5b**, **5c**, **5g**, **5h**, and **5i**

Descriptor	Lipinski	5b	5c	5g	5h	5i
Molecular Weight	≤ 500	270.269	284.296	353.237	304.714	358.684
Logarithme P	≤ 5	3.4638	3.8539	4.0332	4.1172	4.6596
Rotatable Bonds	-	5	6	6	5	5
Hydrogen Bond Acceptors	≤ 10	5	5	6	5	5
Hydrogen Bond Donors	≤ 5	2	2	2	2	2
Surface	-	107.405	113.770	130.765	117.708	130.205

The pkCSM tool was used to evaluate the drug-likeness of the compounds **5b**, **5c**, **5g**, **5h**, and **5i**, including their ADME (Absorption, Distribution, Metabolism, Excretion, and Toxicity) in the body, following the method developed by Douglas E. V. Pires.³⁵ Results of the whole ADME parameters are mentioned in supplementary Table S1-S5. Based on the data, the physicochemical properties, such as molecular weight (less than 400 Da) and surface area of the studied molecules, influence their absorption and distribution in the body as important parameters in drug bioavailability. These ligands show high permeability across Caco-2 cells (with values greater than 0.9, except for compound **5g**) and significant intestinal absorption (ranging from 83.87 % to 88.10 %). These derivatives also demonstrate slightly improved skin permeability, with skin permeability values ranging from -1.022 to 0.225, indicating that some compounds may penetrate the skin. Regarding the blood-brain barrier, benzimidazole derivatives have blood-brain barrier permeability rates between -1.022 and 0.225, suggesting that they do not easily cross this barrier, which limits potential side effects on the brain. The

compounds are also not substrates of CYP2D6/CYP3A4 not inhibitors, except for compound **5g**, which may be metabolized by CYP3A4. Additionally, they are likely not inhibitors of CYP2C9 and CYP2D6. The studied compounds are not expected to be substrates of the renal transporter OCT2, with total clearance ranging from 0.288 to 0.612 log ml/min/kg. However, toxicity analysis shows that compound **5g** might be carcinogenic, and the tested products could cause skin sensitivity and hepatotoxicity, suggesting potential side effects on the liver. Despite these effects, the majority of ADMET parameters are satisfactory, making these derivatives potential candidates for chemotherapy, with side effects to be monitored.

2.3.2 Molecular Docking Study

Our object is to investigate the stability of the five powerful compounds **5b**, **5c**, **5g**, **5h**, and **5i** within the target proteins (strains) involved in antimicrobial activities and to identify the prevalent modes of interaction between these ligands and the crystal structure of the proteins receptors by conducting molecular docking simulations using AutoDock Vina program.³⁶ The most effective drug is the one with the lowest negative binding affinity.

i. Study of the activity of the compound **5g** with *Candida albicans* (Ligand-4ydo interaction study)

The results of this study show that the protein-ligand **5g** complex exhibited an excellent binding affinity with a score of -7.7 kcal/mol, surpassing the reference compound *Fluconazole*, which scored -7.3 kcal/mol (Table S6). Therefore, it follows that ligand **5g** (Diethyl (5-nitro-2-trifluoromethyl-2,3-dihydro-1*H*-benzimidazol-2-yl)phosphonate) stands out as the most effective inhibitor of *Candida albicans*.

The obtained visual analysis of the molecular docking results with **5g** reveals that this ligand penetrates the active site of the protein 4ydo and exhibits strong Hydrogen interactions with the amino acids GLN110, CYS294, and MET308 at a distance of 2.77, 2.76, and 2.31 Å, respectively. As a result, this interaction helps to strengthen the bond between ligand **5g** and 4ydo, enabling the ligand to exert effectively its activity. Additionally, the trifluoromethyl group contained in this compound leads to the formation of a Halogen-Hydrogen interaction with the amino acid MET308 at a distance of 3.04 Å (Fig. 2). This interaction can be explained by the specific physicochemical and biological properties of the fluorine atom, giving the target protein a potentially increased affinity (-7.7 kcal/mol) compared with other compounds and surpassing the reference (*Fluconazole*). These outcomes confirm the greater biological activity of compound **5g** against *Candida albicans*. The other formed complexes (**5b**, **5c**, **5h**, and **5i**) as well as standard stabilize within 4ydo through these interactions and more others; such as hydrophobic and electrostatic interactions via π -alkyl and π -cation bonds, also Pi-Donor Hydrogen bond and Carbon-Hydrogen bond were established and described in supplementary Table S6 and Fig. S1-S5.

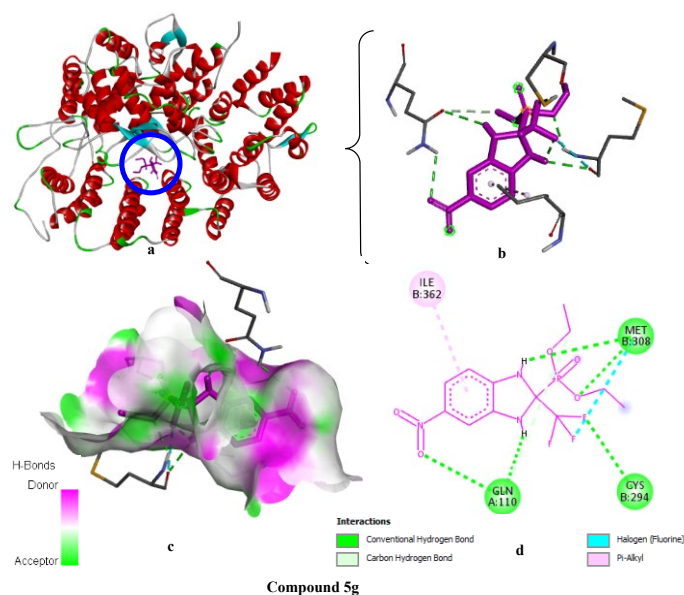


Fig. 2. a: Position of ligand **5g** within the active site of 4ydo and b, c, d: Shows 2D and 3D visualization of the interactions between ligand **5g** and the amino acids of 4ydo, as well as the nature of these interactions

ii. Study of the activity of the compound **5g** with *Escherichia coli* (Ligand-6gj1 interaction study)

With the *Escherichia coli* strain, the results show that compound **5g** demonstrated a binding affinity of -7.7 kcal/mol compared with the reference compound, *Ciprofloxacin*, with a score of -7.9 kcal/mol. Therefore, it follows that ligand **5g** stands out as the closest inhibitor to *Ciprofloxacin*.

As it was the most effective inhibitor (-7.7 kcal/mol), compound **5g** penetrates the active site of the protein 6gj1 and formed four conventional Hydrogen bonds with ASN474, VAL284, and ARG289 with distances ranging from 1.91 Å to 2.70 Å. Additionally, four Halogen (fluorine) interactions via amino acids MET187 and LEU164 were also observed for the same compound. Furthermore, this ligand shaped the carbon-hydrogen bond interaction involving the amino acid GLY471. Moreover, alkyl hydrophobic interaction was observed with amino acid PRO190 (distance: 4.18 Å). These results explain the most important affinity of this compound for protein 6gj1 and corroborate its biological activity against *Escherichia coli*. **Fig. 3** illustrates the various molecular interactions between this inhibitor (**5g**) and the amino acids at the active sites of the protein 6gj1. The visual analysis of the molecular docking results with other ligands **5b**, **5h**, and **5i** as well as the reference compound (*Ciprofloxacin*), reveals that the formed complexes are stabilized within 6gj1 by various important interactions established between these inhibitors and respective target proteins (supplementary **Table S7** and **Fig. S6-S9**).

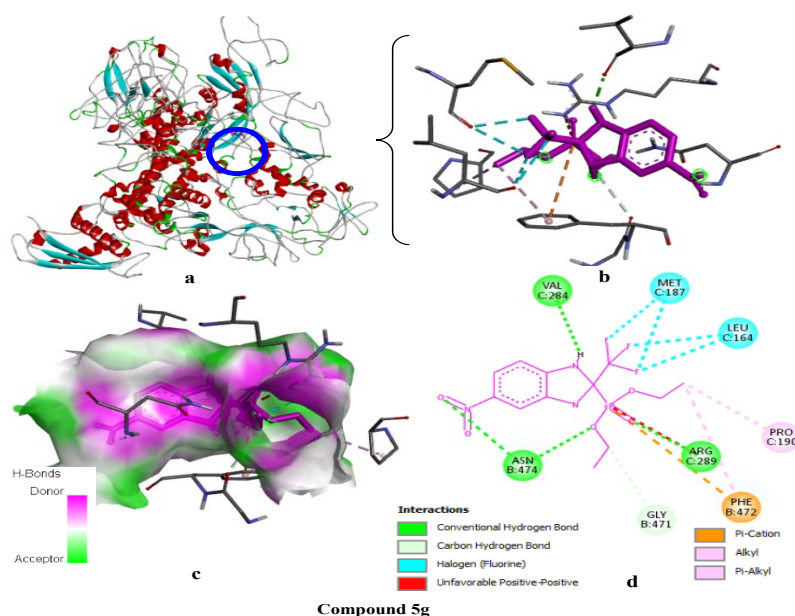


Fig. 3. a: Position of ligand **5g** within the active site of 6gj1 and b, c, d: Shows the 2D and 3D visualization of the interactions between ligand **5g** and the amino acids of 6gj1, as well as the nature of these interactions

iii. Study of the activity of the compounds **5g** and **5i** with *Pseudomonas aeruginosa* (Ligand-7xg0 interaction study)

The docking scores interaction modes shown in Table S8 reveal that compounds **5g** and **5i** displayed the same binding affinity of -7.2 kcal/mol compared with *Ciprofloxacin* which scored -7.9 kcal/mol. It follows that ligands **5g** and **5i** stand out as the most effective inhibitors against *Pseudomonas aeruginosa*.

The visual analysis of the molecular docking results with inhibitors (**5g** and **5i**) explains their higher affinity for *Pseudomonas aeruginosa* protein. For compound **5g**, the formed complex is stabilized within the active sites of the protein 7xg0 by five conventional Hydrogen bonds with amino acids ARG71, ARG75, ASN187, and ASN68 with distances ranging from 2.60 to 3.07 Å. Furthermore, amino acid residues ARG71 and ASN68 are involved in establishing three halogen (fluorine) interactions (distances: 2.91-3.70 Å), as well as three conventional Hydrogen bond Fluorine interactions with amino acids ARG71 and ARG75 (distances: 1.94 – 2.32 Å). It also forms an unfavorable positive charge interaction with amino acid ARG75 (distance: 4.35 Å). These results can be explained by the presence of heteroatoms in the **5g** structure, enabling the complex to be stabilized by the formed hydrogen bond. On the other hand, compound **5i** formed four conventional hydrogen bond interactions with amino acids ARG44, THR69, and SER15. Moreover, classical Hydrogen bond interactions with distances of 2.22 Å and 2.85 Å, were also observed, with amino acids ARG44 and ARG180, respectively. Additionally, unfavorable positive charge interaction involving amino acid ARG180 was also observed for compound **5i** (supplementary Table S8 and Fig. 4 and 5). For the other formed complexes (**5b** and **5h**) as well as the reference compound, the visualization of molecular interactions within the active sites of 7xg0 are elucidated in Fig. S10-S12.

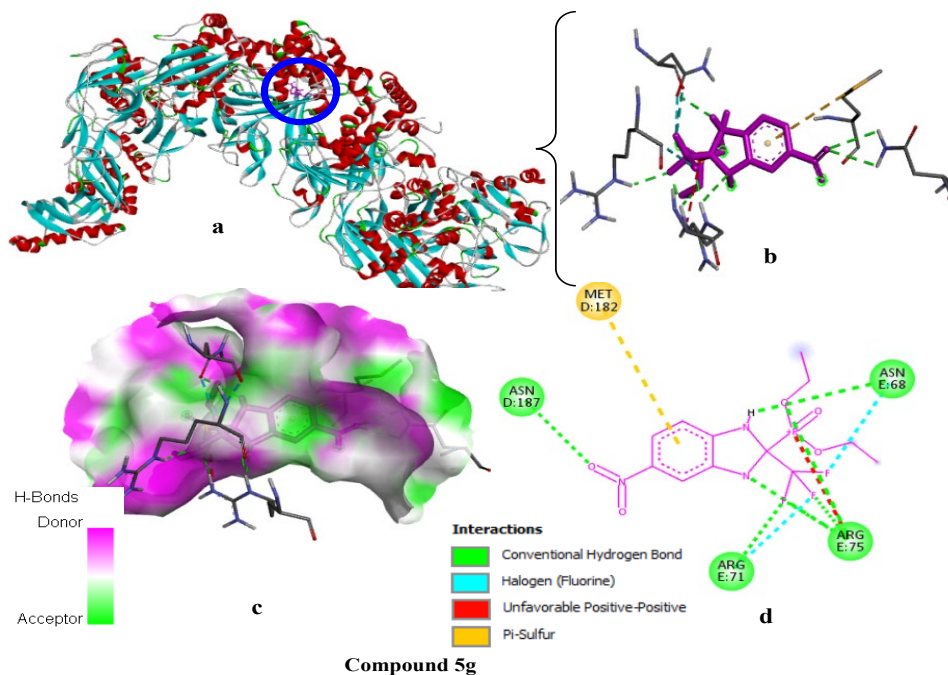


Fig. 4. a: Position of ligand **5g** within the active site of 7xg0 and b, c, d: Shows the 2D and 3D visualization of the interactions between ligand **5g** and the amino acids of 7xg0, as well as the nature of these interactions

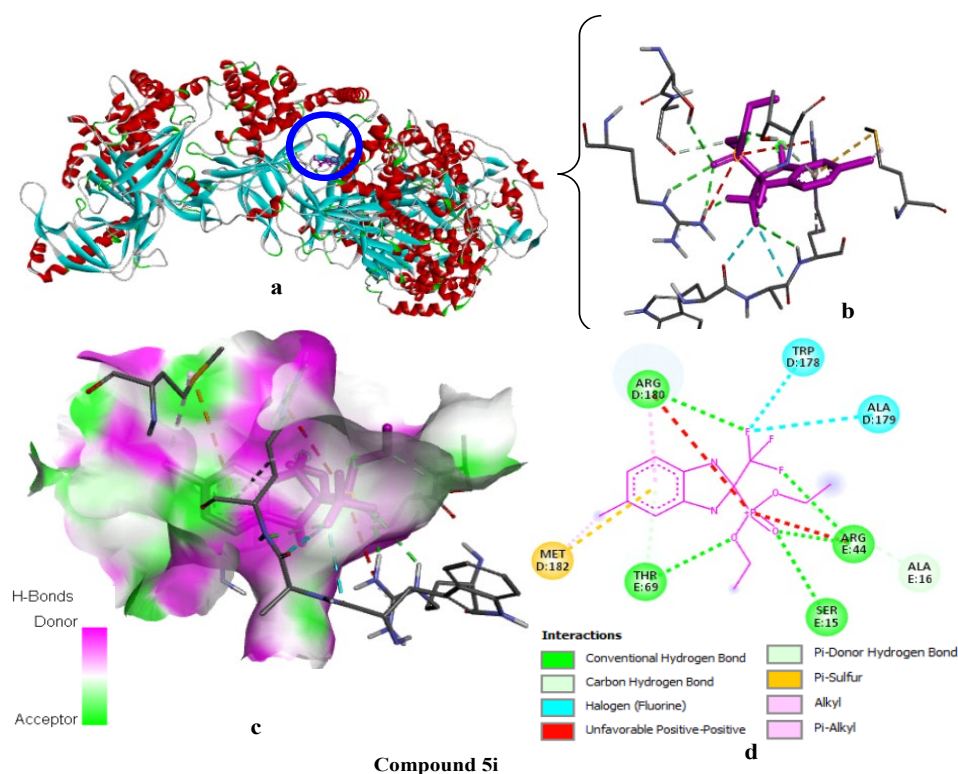


Fig. 5. a: Position of ligand **5i** within the active site of 7xg0 and b, c, d: Shows the 2D and 3D visualization of the interactions between ligand **5i** and the amino acids of 7xg0, as well as the nature of these interactions

iv. Study of the activity of the compound **5g** with *Staphylococcus aureus* (Ligand-5cdp interaction study)

The results, provided in supplementary Table S9, of this study indicate that the protein-ligand **5g** complex was the most effective inhibitor against *Staphylococcus aureus*, with a significant energy value of -8.3 kcal/mol, compared with *Ciprofloxacin* which had a score of -8.4 kcal/mol.

The analysis of the molecular docking results with ligand **5g** explains its higher affinity for the *Staphylococcus aureus* protein. The formed complex is stabilized within the active site of 5cdp by five conventional Hydrogen bonds, provided by

heteroatoms, with amino acids ARG122, SER438, and GLU435, with distances ranging from 1.99 to 2.78 Å. Furthermore, ligand **5g** established six attractive charge interactions with amino acids GLU435, ASP508, and ASP510, as well as four halogen (fluorine) interactions involving amino acid GLU435 (distances: 3.18–3.34 Å). It also formed three Carbon-Hydrogen bonds with ASP508, ASP510, and GLY459, and a Pi-Alkyl interaction as well as a Pi-Pi T-shaped interaction with PHE123 (**Fig. 6**). For other ligands **5b**, **5h**, and **5i** as well as the reference compound, the visualization of the molecular interactions shows that the formed complexes are stabilized within 5cdp by crucial interactions established with the target protein (supplementary **Table S9** and **Fig. S13-S16**).

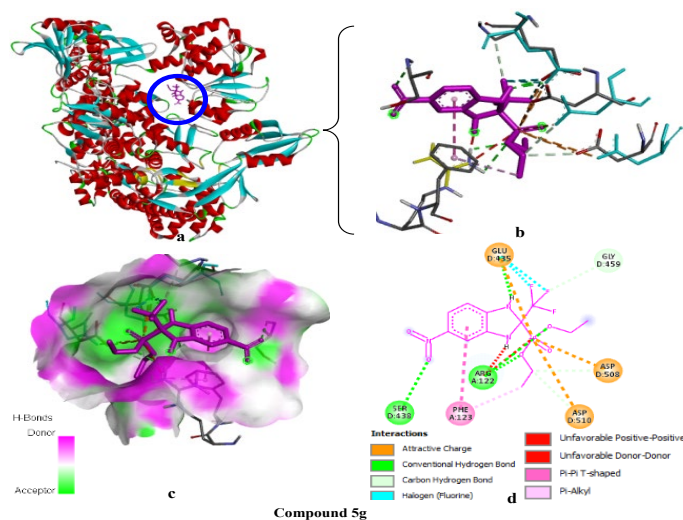


Fig. 6. a: Position of ligand **5g** within the active site of 5cdp and b, c, d: Shows the 2D and 3D visualization of the interactions between ligand **5g** and the amino acids of 5cdp, as well as the nature of these interactions

All the formed interactions between the effective compounds and their respective target proteins emphasize the stabilization of these inhibitors within the active sites of the proteins by explaining their binding modes, resulting in enhanced antimicrobial behavior, in line with the obtained biological results.

2.3.3 DFT Analysis

i. Molecular geometry

Density Functional Theory (DFT) is by far the most widely used method for the precise study of large molecular systems. It enables efficient prediction of molecular properties from the geometry of a molecule.^{37,38} In this work, DFT calculations at the B3LYP level with the 6-31G+(d,p) basis set have been applied to determine the optimal geometries of five compounds presented in **Fig. 7**. All these optimized structures are minima in the potential energy surface (positive frequencies). The total energy values in **Fig. 7** allow us to classify the stability of these compounds as follows: **5i** > **5g** > **5h** > **5c** > **5b**.

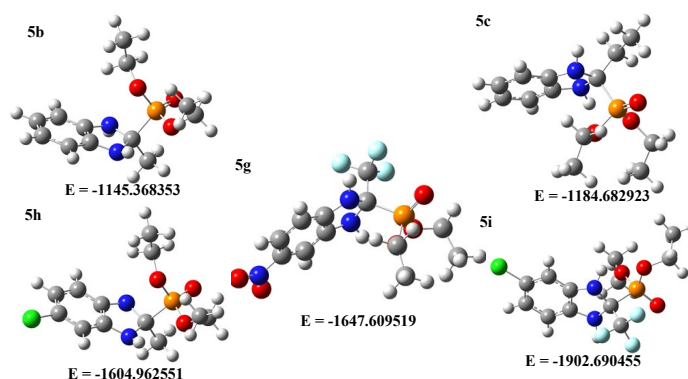


Fig. 7. Optimized structure of compounds **5b**, **5c**, **5g**, **5h**, and **5i** by DFT at the B3LYP/6-31+G(d,p) level

ii. Molecular Electrostatic Potential Surface (MEPS)

Molecular electrostatic potential (MEP) is one of the methods used to identify reactive sites, charge distribution, and hydrogen bonding interactions in a molecule.³⁹ By mapping potential values on the surface of a molecule, the most

electronegative areas in red are associated with electrophilic attack sites, while the most electropositive areas in blue serve as nucleophilic attack sites. Green, yellow, or orange regions correspond to intermediate potentials in ascending order: red < orange < yellow < green < blue.⁴⁰ In this study, the MEP maps in **Fig. 8** clearly show that the oxygen of the P=O bond is a region vulnerable to electrophilic attack (red regions), while the NH amine groups of the imidazole core are nucleophilic attack sites (blue regions). Scanning of each MEP map identifies the aromatic ring centers of five compounds, with chlorine atoms (Cl) in **5h** and **5i** and fluorine atoms (CF₃) in **5g** and **5i** in regions of slightly negative electrostatic potential (orange-yellow), and the nitro group (NO₂) in **5g** in regions of strongly negative electrostatic potential (blue). As a result, all five compounds can establish intermolecular interactions with amino acid residues of target proteins, including donor or acceptor hydrogen bonds, halogen bonds, and hydrophobic bonds.⁴¹

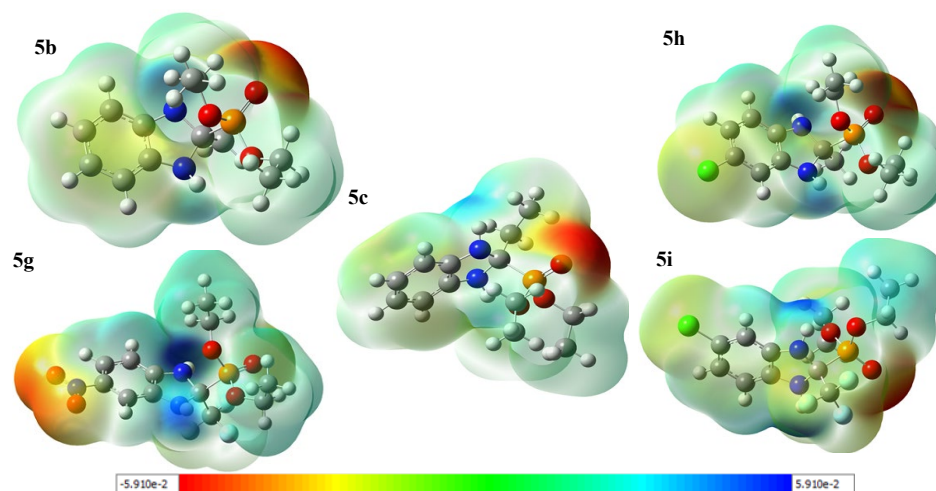


Fig. 8. MEP formed by mapping the total density to the electrostatic potential in the gas phase for compounds **5b**, **5c**, **5g**, **5h**, and **5i**

3. Conclusion

In this work, we described the synthesis of new benzimidazole phosphonates and bisphosphonates with satisfactory yields from differently substituted benzimidazoles and triethyl phosphite using a facile and efficient approach. To the best of our knowledge, this methodology is the first strategy for achieving direct C-P bond construction on the cyclic imine of benzimidazoles. This method has the advantage of being carried out with fewer chemicals under solvent-free conditions, and without any catalyst. The best results were obtained at 80 °C and for 24 hours as the optimized reaction conditions. Synthesized compounds' structures were confirmed using spectroscopic techniques including IR, ¹H-NMR, ¹³C-NMR, and MS. Subsequently, we investigated the antimicrobial activity of the obtained products and we found that certain diethyl benzimidazole phosphonates showed promising results, particularly compounds **5b**, **5g**, **5h**, and **5i** which exhibited notable inhibition against tested pathogenic bacteria with variable minimum inhibitory concentrations (MICs). Compound **5h** displayed notable inhibition against *E. coli* and *S. aureus*. The same compound revealed good activity against *P. aeruginosa*. Besides, compounds **5h** and **5b** showed excellent activity against *C. albicans*. Moreover, these compounds, as well as compounds **5c** and **5g**, displayed excellent action against *Candida albicans*, known for its strong resistance to current antifungal drugs. These findings were therefore complemented by an in-depth investigation of the obtained products' antimicrobial modes of action to struggle with recent and emerging fungal and bacterial threats. For this reason, computational studies i.e., ADMET, molecular docking, and DFT analysis were evaluated and they revealed that the investigated compounds exhibited promising docking efficiency against the target proteins, especially compound **5g** which displayed significant affinity for all the proteins compared with other effective ligands (**5b**, **5c**, **5h**, and **5i**). Accordingly, the convenient procedure adopted in this work has intriguing promise for synthesizing new potentially active organic compounds. For that, our procedure can be applied to synthesize similar (dihydro-1*H*-benzimidazole) phosphonate derivatives, bearing potential and pharmaceutical interest, by starting from mentioned precursors. To date, the application of our method to other new compounds such as bis-benzimidazoles is still under examination and is the subject of our current work. Hence, this work offers exciting forecasts for the creation of novel antimicrobial agents.

Acknowledgement

The authors acknowledge the Department of Chemistry, Chouaib Doukkali University (El Jadida-Morocco) for providing facilities to carry out this research work, the National Center for Scientific Research and Technical (CNRST) in Rabat for performing spectral analysis of the compounds, the Laboratory of Sustainable Development and Health Research, faculty of sciences and techniques, Cadi Ayyad University (Marrakech- Morocco) for evaluating the biological activities of the synthesized compounds.

4. Experimental

4.1 Materials and Methods

Raw materials, reagents, and solvents were purchased from Sigma-Aldrich. Thin layer chromatography (TLC) was carried out on aluminum-baked Merck 0.2 nm silica gel 60 F254. Revelation was carried out under a UV-visible lamp (at 254 and 365 nm). Flash column chromatography was carried out on silica gel 60 Merck 70-230 mesh ASTM, using a mixture of ethyl acetate-hexane as eluant. Solvents were freshly distilled. IR spectra were recorded on a SHIMADZU 8400S FT-IR spectrophotometer. Melting points were measured in degrees Celsius by a Köfler bench and were uncorrected. The (¹H and ¹³C) NMR spectra were recorded on a JNM-ECZ500R/S1 FT NMR SYSTEM (JEOL) Fourier Transform apparatus (500 MHz for proton and 125 MHz for carbon 13) using deuterated dimethyl sulfoxide (DMSO-d₆) as solvent. Chemical shifts were expressed in parts per million (ppm) downstream of the tetramethyl silane internal standard. High-resolution mass spectrometry was performed on a quadrupole-Orbitrap Ultimate 3000-Exactive plus THERMO instrument, equipped with a CNRST collision cell.

4.2 General procedure

4.2.1 Synthesis of benzimidazole derivatives (3a-j)

Benzimidazole compounds were obtained by reacting 1.6 eq (14.8 mmol) of carboxylic acid **2** with a solution of 1,2-phenylenediamine **1** (9.26 mmol) in 4N hydrochloric acid (28 mL) under reflux for 14 h. The reaction mixture was then cooled to room temperature and the pH value of the mixture was set to 8 with 50 % ammonia solution. The precipitating benzimidazoles thus formed were filtered under vacuum and washed several times with a cold water/ethanol (1/1) mixture, then dried at 80 °C. The crude products were recrystallized from ethanol to obtain solids with high yields.

4.2.2 Synthesis of benzimidazole derivative (3k)

9.26 mmol of urea **2k** was introduced in a round-bottomed flask containing a solution of 1,2-diaminobenzene **1** (9.26 mmol) in 10 mL of n-butanol. The resultant mixture was refluxed for 9 h. While cooling, a crystalline solid was formed and separated by filtration, washed with cold ethanol, and dried to yield pure 2-hydroxybenzimidazole **3k** as a crystalline solid.

4.2.3 Synthesis of α-aminophosphonates (5a-j) and bisphosphonate (5k)

A mixture of benzimidazole **3a-k** (2.7 mmol) and triethyl phosphite **4** (5.4 mmol) was introduced into a sealed tube and heated in a sand bath at 80 °C for 24 h. The progress of the reaction was monitored by TLC. The crude product was obtained in an oily form. Chromatography of the residue on silica gel (elution: Ethyl Acetate-Hexane (1/9)) gives the benzimidazole phosphonates **5a-k** in oily and solid forms with moderate to good yields.

Diethyl (2,3-dihydro-1H-benzimidazol-2-yl)phosphonate (5a)

Yield = 61 %; oil. IR-ATR (cm⁻¹): 1275 (P=O); 1615 (C=C); 2981 (CHaro); 3373 (NH). ¹H NMR (500 MHz, DMSO-d₆): δ= 1.36 (t, 6H; 2CH₃), 4.23 (q, 4H; 2CH₂), 7.20 (m, 1H; CH), 7.57 (m, 2H; 2CHaro), 7.63 (m, 2H; 2CHaro), 8.27 ppm (s, 2H; 2NH); ¹³C NMR (125 MHz, DMSO-d₆): δ= 16.4 (CH₃), 16.5 (CH₃), 59.6 (d, CH-P), 63.6 (CH₂), 63.7 (CH₂), 110.9 (CHaro), 119.7 (CHaro), 122.2 (CHaro), 122.9 (CHaro); 133.9 (Cq); 143.4 (Cq); HRMS (70 eV, ESI⁺): calcd for [M+H]⁺: 257.0976 (C₁₁H₁₇N₂O₃P), found: 257.0487.

Diethyl (2-methyl-2,3-dihydro-1H-benzimidazol-2-yl)phosphonate (5b)

Yield = 58 %; oil. IR-ATR (cm⁻¹): 1275 (P=O); 1615 (C=C); 2981 (CHaro); 3373 (NH). ¹H NMR (500 MHz, DMSO-d₆): δ= 1.19 (td, 6H; 2CH₃), 2.65 (s, 3H; CH₃), 3.96 (dq, 4H; 2CH₂), 6.00 (s, 1H; NH), 7.24 (s, H; NH), 7.30 (m, 4H; CHaro); ¹³C NMR (125 MHz, DMSO-d₆): δ= 16.4 (CH₃), 16.5 (CH₃), 24.6 (CH₃), 63.6 (CH₂), 63.6 (CH₂), 81.0 (Cq), 111.5 (CHaro), 116.6 (CHaro), 123.8 (CHaro), 123.8 (CHaro), 133.5 (Cq), 136.9 (Cq); HRMS (70 eV, ESI⁺): calcd for [M+H]⁺: 271.1133 (C₁₂H₁₉N₂O₃P), found: 271.1076.

Diethyl (2-ethyl-2,3-dihydro-1H-benzimidazol-2-yl)phosphonate (5c)

Yield = 32 %; oil. IR-ATR (cm⁻¹): 972; 1025 (P-O-C); 1244 (P=O); 1644 (C=C); 2983 (CHaro); 3427 (NH); ¹H NMR (500 MHz, DMSO-d₆): δ= 1.02 (t, 3H; CH₃), 1.39 (t, 6H; 2CH₃), 3.54 (m, 2H; CH₂), 4.51 (q, 4H; 2CH₂), 5.92 (s, 1H, NH), 7.03 (s, 1H; NH), 7.62 (m, 2H; 2CHaro), 8.02 ppm (m, 2H; 2CHaro); ¹³C NMR (125 MHz, DMSO-d₆): δ= 12.3 (CH₃), 17.3 (CH₃), 17.4 (CH₃), 40.8 (CH₂), 57.9 (CH₂), 57.9 (CH₂), 113.7 (2CHaro); 126.6 (2CHaro); 131.1 (2Cq); HRMS (70 eV, ESI⁺): calcd for [M+H]⁺: 285.1289 (C₁₃H₂₁N₂O₃P), found: 285.1323.

Diethyl (2,5-dimethyl-2,3-dihydro-1H-benzimidazol-2-yl)phosphonate (5d)

Yield = 48 %; oil. IR-ATR (cm⁻¹): 1281 (P=O); 1621 (C=C); 2922; 2978 (CHaro); 3365 (NH). ¹H NMR (500 MHz, DMSO-d₆): δ= 1.22 (td, 6H; 2CH₃), 2.38 (s, 3H; CH₃), 2.47 (s, 3H; CH₃), 4.11 (qd, 4H; 2CH₂), 6.94 (m, 2H; 2CHaro), 7.23 (m, 1H;

CHaro), 7.36 (s, 1H; NH), 7.37 (s, 1H; NH) ppm; ^{13}C NMR (125 MHz, DMSO- d_6): δ = 15.2 (CH₃), 15.3 (CH₃), 21.6 (CH₃), 21.8 (CH₃), 58.8 (CH₂), 58.9 (CH₂), 60.3 (Cq), 110.0 (CHaro), 118.2 (CHaro), 123.1 (CHaro), 130.7 (Cq), 135.3 (Cq), 140.6 (Cq); HRMS (70 eV, ESI+): calcd for $[\text{M}+\text{H}]^+$: 285.1289 (C₁₃H₂₁N₂O₃P), found: 285.2313.

Diethyl (5-methyl-2-trifluoromethyl-2,3-dihydro-1H-benzimidazol-2-yl)phosphonate (5e)

Yield = 32 %; m.p. 60-62 °C (Ethanol). IR-ATR (cm⁻¹): 1284.5 (P=O); 1621 (C=C); 2932 (CHaro); 2971. ^1H NMR (500 MHz, DMSO- d_6): δ =1.31 (td, 6H; 2CH₃), 2.39 (s, 3H; CH₃), 4.35 (m, 4H; 2CH₂), 7.15 (dd, 1H; CHaro), 7.24 (dd, 1H; CHaro), 7.53 (m, 1H; CHaro), 7.63 (s, 1H; NH), 7.65 ppm (s, 1H; NH); ^{13}C NMR (125 MHz, DMSO- d_6): δ = 15.5 (CH₃), 15.6 (CH₃), 21.6 (CH₃), 41.1 (CH₂), 41.4 (CH₂), 111.5 (d, CHaro), 111.7 (d, CHaro), 119.7 (Cq, $^1\text{J}_{\text{C-F}}$ = 268.7 Hz, CF₃), 120.9 (s, CHaro), 133.4 (Cq), 133.6 (Cq), 135.7 (Cq); RMN ^{19}F (500 MHz, DMSO- d_6): δ = - 61.13 ppm (s, 3F; CF₃); HRMS (70 eV, ESI+): calcd for $[\text{M}+\text{H}]^+$: 339.1007 (C₁₃H₁₈F₃N₂O₃P), found: 339.1962.

Diethyl (5-nitro-2,3-dihydro-1H-benzimidazol-2-yl)phosphonate (5f)

Yield = 21 %; m.p. 120-122 °C (Ethanol). IR-ATR (cm⁻¹): 1283 (P=O); 1614.8 (C=C); 2972 (CHaro); 3099 (NH). ^{13}C NMR (125 MHz, DMSO- d_6): δ = 16.4 (CH₃), 16.5 (CH₃), 57.9 (d, CH-P), 63.6 (CH₂), 63.6 (CH₂), 108.2 (CHaro), 117.6 (CHaro), 120.2 (CHaro), 133.5 (Cq), 143.3 (Cq), 148.4 (Cq); HRMS (70 eV, ESI+): calcd for $[\text{M}+\text{H}]^+$: 302.0827 (C₁₁H₁₆N₃O₅P), found: 302.1260.

Diethyl (5-nitro-2-trifluoromethyl-2,3-dihydro-1H-benzimidazol-2-yl)phosphonate (5g)

Yield = 31 %; m.p. 112-114 °C (Ethanol). IR-ATR (cm⁻¹): 1288 (P=O); 1619 (C=C); 2992 (CHaro); 3096 (NH). ^1H NMR (500 MHz, DMSO- d_6): δ = 1.35 (t, 6H; 2CH₃), 4.46 (q, 4H; 2CH₂), 8.01 (s, 1H; NH), 8.02 (s, 1H; CHaro), 8.25 (m, 2H; 2CHaro), 8.61 ppm (s, 1H; NH); ^{13}C NMR (125 MHz, DMSO- d_6): δ = 15.5 (CH₃), 15.8 (CH₃), 41 (CH₂), 41.1 (CH₂), 88.8 (Cq), 109.7 (CHaro), 113.3 (CHaro), 117.9 (CHaro), 115.8-122.3 (Cq, $^1\text{J}_{\text{C-F}}$ = 270 Hz, CF₃), 134.9 (Cq), 139.5 (Cq), 140.1 (Cq); RMN ^{19}F (500 MHz, DMSO- d_6): δ = - 62.05 ppm (s, 3F; CF₃); HRMS (70 eV, ESI+): calcd for $[\text{M}+\text{H}]^+$: 371.0701 (C₁₂H₁₅F₃N₃O₅P), found: 371.0102.

Diethyl (5-chloro-2-methyl-2,3-dihydro-1H-benzimidazol-2-yl)phosphonate (5h)

Yield = 62 %; oil. IR-ATR (cm⁻¹): 1276 (P=O); 1609 (C=C); 1708; 2935; 2979 (CHaro). ^1H NMR (500 MHz, DMSO- d_6): δ = 1.19 (t, 6H; 2CH₃), 2.49 (s, 3H; CH₃), 4.13 (m, 2H; CH₂), 6.63 (s, 1H; NH), 7.12 (m, 2H; 2CHaro), 7.44 (m, 1H; CHaro), 7.48 ppm (m, 1H; NH); ^{13}C NMR (125 MHz, DMSO- d_6): δ = 16.7 (CH₃), 16.8 (CH₃), 21.6 (CH₃), 61.3 (CH₂), 61.4 (CH₂), 110.4 (CHaro), 111.5 (CHaro), 122.1 (CHaro), 126.4 (Cq), 133.8 (Cq), 135.7 ppm (Cq); HRMS (70 eV, ESI+): calcd for $[\text{M}-\text{H}]^-$: 303.0743 (C₁₂H₁₈ClN₂O₃P), found: 303.0635.

Diethyl (5-chloro-2-trifluoromethyl-2,3-dihydro-1H-benzimidazol-2-yl)phosphonate (5i)

Yield = 55 %; m.p. 86-88 °C (Ethanol). IR-ATR (cm⁻¹): 1286 (P=O); 1580 (C=C); 2969 (CHaro). ^1H NMR (500 MHz, DMSO- d_6): δ =1.33 (td, 6H; 2CH₃), 4.41 (qd, 4H; 2CH₂), 7.48 (dd, 2H; 2CHaro), 7.84 (s, 1H; NH), 7.85 (s, 1H; NH), 7.89 ppm (d, 1H; CHaro); ^{13}C NMR (125 MHz, DMSO- d_6): δ = 15.6 (CH₃), 15.7 (CH₃), 40.6 (CH₂), 40.7 (CH₂), 112.4 (Cq), 113.9 (CHaro), 116.1-122.6 (Cq, $^1\text{J}_{\text{C-F}}$ = 270 Hz, CF₃), 120.8 (CHaro), 126.2 (CHaro), 128.6 (Cq), 134.3 (Cq), 134.4 ppm (Cq); RMN ^{19}F (500 MHz, DMSO- d_6): δ = - 61.45 ppm (s, 3F; CF₃); HRMS (70 eV, ESI+): calcd for $[\text{M}+\text{H}]^+$: 359.0460 (C₁₂H₁₅ClF₃N₂O₃P), found: 359.1619.

Diethyl (5-bromo-2-methyl-2,3-dihydro-1H-benzimidazol-2-yl)phosphonate (5j)

Yield = 16 %; m.p. 262-264 °C (Ethanol). IR-ATR (cm⁻¹): 963; 1044 (P-O-C); 1246 (P=O); 1610 (C=C); 2929; 2979 (CHaro); 3389 (NH). ^1H NMR (500 MHz, DMSO- d_6): δ = 1.33 (td, 6H; 2CH₃), 2.9 (s, 3H; CH₃), 4.49 (qd, 4H; 2CH₂), 5.9 (s, 1H; NH), 7.04 (s, 1H; NH), 7.75 (d, 1H; CHaro), 8.01 (d, 1H; CHaro), 8.39 ppm (s, 1H; CHaro); ^{13}C NMR (125 MHz, DMSO- d_6): δ = 14.6 (CH₃), 17.2 (CH₃), 17.3 (CH₃), 58.1 (CH₂), 58.2 (CH₂), 115.3 (CHaro), 116.3 (CHaro), 118.9 (Cq), 129.4 (CHaro), 130.3 (Cq), 132.2 (Cq); HRMS (70 eV, ESI+): calcd for $[\text{M}+\text{H}]^+$: 350.0217 (C₁₂H₁₈BrN₂O₃P), found: 350.9982.

Tetraethyl (2,3-dihydro-1H-benzimidazol-2,2-diyl)bisphosphonate (5k)

Yield = 50 %; oil. IR-ATR (cm⁻¹): IR-ATR (cm⁻¹): 1018 (P-O-C); 1225 (P=O); 1682 (C=C); 2412; 2937; 2983 (CHaro); 3396 (NH). ^1H NMR (500 MHz, DMSO- d_6): δ = 1.19 (t, 6H; 2CH₃), 1.21 (t, 6H; 2CH₃), 3.94 (q, 4H; 2CH₂), 3.97 (q, 4H; 2CH₂), 7.01 (dd, 2H; 2CHaro), 7.14 ppm (m, 2H; 2CHaro); ^{13}C NMR (125 MHz, DMSO- d_6): δ = 16.4 (2CH₃), 16.5 (2CH₃), 63.6 (2CH₂), 63.6 (2CH₂), 108.3 (2CHaro), 121.3 (2CHaro), 129.2 (2Cq); HRMS (70 eV, ESI+): calcd for $[\text{M}+\text{H}]^+$: 393.1266 (C₁₅H₂₆N₂O₆P₂), found: 393.1508.

4.3 Biological activity

4.3.1 Antimicrobial test

In this study, synthesized compounds were examined *in vitro* for their antibacterial and antifungal activity against three types of microorganisms: *Candida albicans* (ATCC 10231), two Gram-positive bacteria; *Staphylococcus aureus* (*S. aureus*) (ATCC 25923) and *Pseudomonas aeruginosa* (*P. aeruginosa*) (CIP A22), and one Gram-negative bacteria; *Escherichia coli* (*E. coli*) (ATCC 25922). The Pasteur Institute (Casablanca, Morocco) provided the bacterial strains. Before being used, they were kept at + 4 °C and cared for by regular subcultures.

i. Disc diffusion technique

The Agar disc diffusion performance was utilized in agreement with the Mersly et al. protocol.⁴² Sterile 6 mm diameter cellulose discs impregnated with 10 µL of each drug at a concentration of 500 ppm were stacked on top of Mueller-Hinton agar containing 3×10^8 CFU/mL bacteria. The positive control employed in the well was a disk containing the common antibiotic *Ciprofloxacin/Fluconazole* and the negative control was a disc containing DMSO. After incubating the pathogenic bacteria or fungus for 24 h at 37 °C, the inhibitory diameter surrounding the discs in proportion to the common antibiotic was determined in order to do this.

ii. Determination of Minimum Inhibitory Concentration (MIC)

As reported by Anthony et al.,³³ a 96-well microdilution plates were utilized in the microdilution broth experiment to assess the minimum inhibitory concentration (MIC) of the studied products against pathogenic bacteria. Using the double-fold dilution method, a series of solutions were made for each derivative compound in Mueller-Hinton broth, ranging from 1.2 to 1000 µg/mL. Then, the 96-well plates were filled with 100 µL of each sample's solution and 10 µL of the bacterial suspension (tuned at 0.5 McFarland). The plates were then incubated for 24 h at 37 °C. Instead of using chemical solutions, DMSO, ciprofloxacin, and Mueller-Hinton broth were used as positive and negative controls, respectively. Following the incubation period, a measurement at 600 nm was used to calculate the MIC.

4.4 Computational studies

4.4.1 Molecular Docking Study

In order to explain the binding affinity and interactive mode between ligand and selected protein target, the biological activity of the active compounds was assessed using AutoDock Vina³⁶ through the virtual screening tool PyRx 0.8,⁴³ targeting the main protease of *Candida albicans* (PDB id = 7xg0), *Escherichia coli* (PDB id = 6gj1),⁴⁴ *Pseudomonas aeruginosa* (PDB id = 7xg0),⁴⁵ and *Staphylococcus aureus* (PDB id = 5cdp).⁴⁶ AutoDock Tools-1.5.6 was used to prepare the proteins and perform molecular docking.⁴⁷ All proteins' HETATM and water atoms were initially removed, and then polar hydrogens and Kollman charges were added. Finally, the proteins were saved in PDBQT format. The grid was also prepared using this software. The prepared ligands were docked with AutoDock Vina, and the interaction diagrams and binding modes were created using Biovia Discovery Studio 2021 Client.

4.4.2 DFT Analysis

Global chemical reactivity descriptors

DFT is a crucial technique for studying the link between chemical compounds' geometry and electronic characteristics.^{37,38} It uses the electron density of a chemical system to elucidate fundamental concepts concerning chemical reactivity in order to understand the essence of chemical interactions and predict the chemical reactivity of molecules, atoms, or ions.³⁸ In this work, all calculations and product optimizations were performed at the B3LYP level of theory, with a 6-31G+ (d,p) base set, and were generated using Gaussian 09 and Gauss View 5.0.⁴⁸ For this purpose, global chemical descriptors such as HOMO and LUMO, energy gap (ΔE), electronegativity (χ), and reactivity indices, including electronic chemical potential (μ), chemical hardness (η), softness (σ), ionization potential (PI), electronic affinity (EA), global electrophilicity (ω), global nucleophilicity (N), and dipole moment (μ_d) were determined using the following expressions:⁴⁹

$$\Delta E = E_{\text{HOMO}} - E_{\text{LUMO}} \text{ (1)} / \text{IP} = -E_{\text{HOMO}} \text{ and } \text{EA} = -E_{\text{LUMO}} \text{ (2)} / \mu = -1/2(\text{IP} + \text{EA}) \text{ (3)} / \eta = 1/2(\text{IP} - \text{EA}) \text{ (4)} / \omega = \mu^2/2\eta \text{ (5)} / \text{N} = E_{\text{HOMO}(\text{Nu})} - E_{\text{LUMO}(\text{TCE})} \text{ (6)} / \text{S} = 1/\eta \text{ (7)}$$

Declaration of competing interest: The authors declare no conflicts.

Finding: No external funding was received for this research paper.

Data availability statement: No data was used for the research described in the article.

Supplementary materials: Supplementary data supporting the outcomes of this research are available from the corresponding author.

References

- Chaban TI, Klenina OV, Chaban IH, Lelyukh MI. (2024) Recent advances in the synthesis of thiazolo[4,5-b]pyridines. Part 2: Focus on thiazole annulation to pyridine ring (microreview). *Chem. Heterocycl. Compd.*, 60(3):130-132. <https://doi.org/10.1007/s10593-024-03307-1>.
- Lelyukh MI, Komarenska ZM, Chaban TI, Chaban IH. (2024) An overview of the synthetic routes toward [1, 2, 4]thiazolo[3,4-b][1,3,4]thiadiazoles (microreview). *Chem. Heterocycl. Compd.*, 60(7):342-344. <https://doi.org/10.1007/s10593-024-03343-x>.
- Prakash C, Singh R. (2024) Synthesis of fluorinated six-membered nitrogen heterocycles using microwave irradiation. *Chem. Heterocycl. Compd.*, 60(5):216-229. <https://doi.org/10.1007/s10593-024-03323-1>.
- Zhilitskaya LV, Yarosh NO. (2024) The synthesis of salts of five-membered heterocyclic compounds based on N-containing cations/anions (microreview). *Chem. Heterocycl. Compd.*, 60(5):230-232. <https://doi.org/10.1007/s10593-024-03324-0>.
- Marinescu, M.; Cinteza, L. O.; Marton, G. I.; Chifiriuc, M.-C.; Popa, M.; Stanculescu, I.; Zălaru, C.-M.; Stavarache, C.-E. (2020) Synthesis, Density Functional Theory Study and in Vitro Antimicrobial Evaluation of New Benzimidazole Mannich Bases. *BMC Chem.*, 14 (1), 45. <https://doi.org/10.1186/s13065-020-00697-z>.
- Bistrović, A.; Krstulović, L.; Stolić, I.; Drenjančević, D.; Talapko, J.; Taylor, M. C.; Kelly, J. M.; Bajić, M.; Raić-Malić, S. (2018) Synthesis, Anti-Bacterial and Anti-Protozoal Activities of Amidinobenzimidazole Derivatives and Their Interactions with DNA and RNA. *J. Enzyme Inhib. Med. Chem.*, 33 (1), 1323–1334. <https://doi.org/10.1080/14756366.2018.1484733>.
- Kenchappa, R.; Bodke, Y. D.; Telkar, S.; Aruna Sindhe, M. (2017) Antifungal and anthelmintic activity of novel benzofuran derivatives containing thiazolo benzimidazole nucleus: an in vitro evaluation. *J. Chem. Bio.*, 10(1), 11–23. <https://doi.org/10.1007/s12154-016-0160-x>.
- Argirova, M. A.; Georgieva, M. K.; Hristova-Avakumova, N. G.; Vuchev, D. I.; Popova-Daskalova, G. V.; K.; Anichina, K.; Yancheva, D. Y. (2021) New 1H-benzimidazole-2-yl hydrazones with combined antiparasitic and antioxidant activity. *RSC Adv.*, 11, 39848. <https://doi.org/10.1039/d1ra07419a>.
- Hwu, J. R.; Singha, R.; Hong, S. C.; Chang, Y. H.; Das, A. R.; Vliegen, I.; De Clercq, E.; Neyts, J. (2008) Synthesis of New Benzimidazole–Coumarin Conjugates as Anti-Hepatitis C Virus Agents. *Antiviral Res.*, 77 (2), 157–162. <https://doi.org/10.1016/j.antiviral.2007.09.003>.
- Tremblay, M. et al. (2012) Inhibition of HIV-1 capsid assembly: Optimization of the antiviral potency by site selective modifications at N1, C2 and C16 of a 5-(5-furan-2-yl-pyrazol-1-yl)-1H-benzimidazole scaffold. *Bioorg. Med. Chem. Lett.*, 22(24), 7512–7517. <https://doi.org/10.1016/j.bmcl.2012.10.034>.
- Raka, S. C.; Rahman, A.; Hussain, F.; Abdur Rahman, S. M. (2022) Synthesis, Characterization and in Vitro, in Vivo, in Silico Biological Evaluations of Substituted Benzimidazole Derivatives. *Saudi J. Biol. Sci.*, 29 (1), 239–250. <https://doi.org/10.1016/j.sjbs.2021.08.082>.
- Shiyang, Z. and Gangliang, H. (2020) Synthesis of anti-allergic drugs. *RSC Adv.*, 10, 5874-5885. <https://doi.org/10.1039/C9RA10659F>.
- Yalcin-Ozkat, G. et al. (2023) Design, synthesis, and computational studies of benzimidazole derivatives as new antitubercular agents, *J. Biomol. Struct. Dyn.*, 41, 7. <https://doi.org/10.1080/07391102.2022.2036241>.
- Sahariah, M.; Chowdhury, R.; Pegu, P. et al. (2024) Design, synthesis and in-vitro anti-depressant activity evaluation of some 2-styrylbenzimidazole derivatives. *Futur. J. Pharm. Sci.*, 10, 20. <https://doi.org/10.1186/s43094-024-00589-2>.
- Sethy, S.; Mandal, S. K.; Ewies, E. F.; Dhiman, N.; Garg, A. (2021) Synthesis, Characterization and Biological Evaluation of Benzimidazole and Benzindazole Derivatives as Anti-Hypertensive Agents. *Egypt. J. Chem.*, 64 (7), 3659–3664. <https://doi.org/10.21608/ejchem.2021.79840.3931>.
- Gümrukçüoğlu, N. (2021) Synthesis and Antioxidant Properties of New Benzimidazole Derivatives. *J. Polytech.*, 24 (4), 1699–1706. <https://doi.org/10.2339/politeknik.718979>.
- Satiya, G.; Sharma, B.; Madan, A.; Iqbal, A.; Shaquiquzzaman, M.; Akhter, M.; Parvez, S.; Khan, M. A.; Alam, M. M. (2022) Benzimidazole Based Derivatives as Anticancer Agents: Structure Activity Relationship Analysis for Various Targets. *J. Heterocycl. Chem.*, 59 (1), 22–66. <https://doi.org/10.1002/jhet.4355>.
- Abouelhaoul, E. A.; El Kihel, A.; Ahabala, M.; Sdassi, H.; Köhler, L. H. F.; Bauchat, P.; Roisnel, T.; Khan, T. A.; Al Nasr, I. S.; Koko, W. S.; Schobert, R.; Biersack, B. (2023) Regiospecific Reduction of 4,6-Dinitrobenzimidazoles: Synthesis, Characterization, and Biological Evaluation. *Chem. Biodivers.*, 20 (7), e202300191. <https://doi.org/10.1002/cbdv.202300191>.
- Quin, L. D. (2000) A Guide to Organophosphorus Chemistry; John Wiley & Sons.
- Kufelnicki, A.; Woźniczka, M.; Kalinowska-Lis, U.; Jezierska, J.; Ochocki, J. (2013) Synthesis, Acid–Base and Complexing Properties with Cu(II), Co(II) and Zn(II) in Aqueous Solution of a Novel 1H-Benzimidazol-2-Ylmethyl Diethyl Phosphate Ligand: Comparison with Other 2-Substituted Benzimidazole Ligands. *Polyhedron*, 53, 20–25. <https://doi.org/10.1016/j.poly.2013.01.006>.
- Sánchez-Moreno, M. J.; Gómez-Coca, R. B.; Fernández-Botello, A.; Ochocki, J.; Kotynski, A.; Griesser, R.; Sigel, H. (2003) Synthesis and Acid–Base Properties of (1H-Benzimidazol-2-Yl-Methyl)Phosphonate (Bimp2–). Evidence for

- Intramolecular Hydrogen-Bond Formation in Aqueous Solution between (N-1) H and the Phosphonate Group. *Org. Biomol. Chem.*, 1 (10), 1819–1826. <https://doi.org/10.1039/B301281F>.
- 22 Sánchez-Moreno, M. J.; Fernández-Botello, A.; Gómez-Coca, R. B.; Griesser, R.; Ochocki, J.; Kotynski, A.; Niclós-Gutiérrez, J.; Moreno, V.; Sigel, H. (2004) Metal Ion-Binding Properties of (1H-Benzimidazol-2-Yl-Methyl)Phosphonate (Bimp2-) in Aqueous Solution. Isomeric Equilibria, Extent of Chelation, and a New Quantification Method for the Chelate Effect. *Inorg. Chem.*, 43 (4), 1311–1322. <https://doi.org/10.1021/ic030175k>.
- 23 Tverdomed, S. N.; Kolanowski, J.; Lork, E.; Rösenthaller, G.-V. (2011) An effective synthetic route to ortho difluoromethyl arylphosphonates: studies on the reactivity of phosphorus- and fluorine-containing functions. *Tetrahedron*, 67(21), 3887–3903. <https://doi.org/10.1016/j.tet.2011.03.076>.
- 24 Kalinowska-Lis, U.; Szewczyk, E. M.; Chęcińska, L.; Wojciechowski, J. M.; Wolf, W. M.; Ochocki, J. (2014) Synthesis, Characterization, and Antimicrobial Activity of Silver(I) and Copper (II) Complexes of Phosphate Derivatives of Pyridine And Benzimidazole. *Chem. Med. Chem.*, 9 (1), 169–176. <https://doi.org/10.1002/cmdc.201300333>.
- 25 Ali, T. E. (2014) Synthetic Methods of Cyclic α -Aminophosphonic Acids and Their Esters. *Arkivoc*, (1), 21–91. <https://doi.org/10.3998/ark.5550190.p008.189>.
- 26 Phillips, M. A. CCCXVII.—(1928) The Formation of 2-Substituted Benzimidazoles. *J. Chem. Soc.*, No. 0, 2393–2399. <https://doi.org/10.1039/JR9280002393>.
- 27 Mavrova, A.; Anichina, K.; Izevbehai, O.; Vuchev, D.; Popova, G.; Yancheva, D.; Stoyanov, S. (2021) New 1,3-disubstituted benzimidazol-2-ones as a promising scaffold for the antitrihinellosis agents development. *J. Chem. Techn. Metallurg.*, 56, 1, 3–9.
- 28 Castejon-Flores, J. L.; Guevara-Moreno, O. E.; Díaz-Contreras, R. R.; Gutiérrez-Carrillo, A.; Franco-Pérez, M.; Suárez-Moreno, G. V.; Zamudio-Medina, A. (2019) Multicomponent One-Pot Synthesis of (Dihydro-1H-Benzo[d]Imidazole) Phosphonate. *Phosphorus Sulfur Silicon Relat. Elem.*, 194 (11), 1062–1066. <https://doi.org/10.1080/10426507.2019.1602834>.
- 29 Johnson, F. E.; Cabasso, I. (2010) Synthesis and Mechanism of PBI Phosphonate, Poly[2,2'-(m-Phenylene)-5,5'-Bibenzimidazole Phosphonate Ester], and Its Polyphosphonic Acid Derivatives. *Macromolecules*, 43 (8), 3634–3651. <https://doi.org/10.1021/ma100320w>.
- 30 Odinets, I. L.; Artyushin, Oleg. I.; Lyssenko, K. A.; Shevchenko, N. E.; Nenajdenko, V. G.; Rösenthaller, G.-V. (2009) Facile Synthesis of Cyclic α -Perfluoroalkyl- α -Aminophosphonates. *J. Fluor. Chem.*, 130 (7), 662–666. <https://doi.org/10.1016/j.jfluchem.2009.05.002>.
- 31 Sabry, E.; Abu Bakr, S. M.; Khidre, M. D.; Awad, H. M.; Sediek, A. A. (2024) Synthesis, Characterization and Antitumor Activity of Benzimidazole Phosphonate Derivatives. *Egypt. J. Chem.*, 67 (13), 443–452. <https://doi.org/10.21608/ejchem.2024.257129.9050>.
- 32 Lee, Y.; Puumala, E.; Robbins, N.; Cowen, L. E. (2021) Antifungal Drug Resistance: Molecular Mechanisms in *Candida Albicans* and Beyond. *Chem. Rev.*, 121 (6), 3390–3411. <https://doi.org/10.1021/acs.chemrev.0c00199>.
- 33 Anthony, K. B.; Fishman, N. O.; Linkin, D. R.; Gasink, L. B.; Edelstein, P. H.; Lautenbach, E. (2008) Clinical and Microbiological Outcomes of Serious Infections with Multidrug-Resistant Gram-Negative Organisms Treated with Tigecycline. *Clin. Infect. Dis.*, 46 (4), 567–570. <https://doi.org/10.1086/526775>.
- 34 Chandran, K.; Shane, D. I.; Zochedh, A.; Sultan, A. B.; Kathiresan, T. (2022) Docking Simulation and ADMET Prediction Based Investigation on the Phytochemical Constituents of Noni (*Morinda Citrifolia*) Fruit as a Potential Anticancer Drug. *In Silico Pharmacol.*, 10 (1), 14. <https://doi.org/10.1007/s40203-022-00130-4>.
- 35 Pires, D. E. V.; Blundell, T. L.; Ascher, D. B. (2015) pkCSM: Predicting Small-Molecule Pharmacokinetic and Toxicity Properties Using Graph-Based Signatures. *J. Med. Chem.*, 58 (9), 4066–4072. <https://doi.org/10.1021/acs.jmedchem.5b00104>.
- 36 Trott, O.; Olson, A. J. (2010) AutoDock Vina: Improving the Speed and Accuracy of Docking with a New Scoring Function, Efficient Optimization, and Multithreading. *J. Comput. Chem.*, 31 (2), 455–461. <https://doi.org/10.1002/jcc.21334>.
- 37 Majumdar, D.; Pal, T. K.; Sakib, S. A.; Das, S.; Bankura, K.; Mishra, D. (2021) Synthesis, spectroscopic characterization, and SC-XRD study of one privileged heteronuclear Ni(II)/Hg(II)-Salen complex: An exclusive DFT outlook. *Inorg. Chem. Commun.*, 128, 108609. <https://doi.org/10.1016/j.inoche.2021.108609>.
- 38 Majumdar, D.; Dubey, A.; Tufail, A.; Sutradhar, D.; Roy, S. (2023) Synthesis, Spectroscopic Investigation, Molecular Docking, ADME/T Toxicity Predictions, and DFT Study of Two Trendy Ortho Vanillin-Based Scaffolds. *Heliyon*, 9 (6), e16057. <https://doi.org/10.1016/j.heliyon.2023.e16057>.
- 39 Lohith, T.N. et al. (2022) N-[2-(5-bromo-2-chloro-pyrimidin-4-yl)thio]-4-methoxy-phenyl]-4-chlorobenzenesulfonamide: The existence of H-bond and halogen bond interactions assisted supramolecular architecture – A quantum chemical investigation. *J. Mol. Struct.*, 1267, 133476. <https://doi.org/10.1016/j.molstruc.2022.133476>.
- 40 Ali, O. A. A.; Elangovan, N.; Mahmoud, S. F.; El-Gendey, M. S.; Elbasheer, H.; El-Bahy, S. M.; Thomas, R. (2022) Synthesis, Characterization, Vibrational Analysis and Computational Studies of a New Schiff Base from Pentafluoro Benzaldehyde and Sulfanilamide. *J. Mol. Struct.*, 1265, 133445. <https://doi.org/10.1016/j.molstruc.2022.133445>.
- 41 Neetha, S.; Lohith, T. N.; Santhosh, C.; Sheela, K.; Ravi Singh, K.; Sridhar, M. A.; Sadashiva, M.P. (2024) A Comprehensive Analysis of the Molecular Packing in the Crystal of (4-Methoxyphenyl)methyl 4-(4-Chlorophenyl)-1,3-Thiazole-2-Carboxylate: Insights of X-Ray Crystallography and DFT Analysis. *J. Mol. Struct.*, 1319, 139584. <https://doi.org/10.1016/j.molstruc.2024.139584>.

- 42 EL Mersly, L.; EL Mouchtari, E. M.; Zefzoufi, M.; Sarakha, M.; EL Haddad, M.; Rafqah, S. (2022) Kinetics, Mechanism Studies and Antibacterial Activity of Pharmaceutical Sulfaguanidine under Light Irradiation in Aqueous Solution. *J. Photochem. Photobiol. A Chem.*, 430, 113985. <https://doi.org/10.1016/j.jphotochem.2022.113985>.
- 43 Dallakyan, S.; Olson, A. J. (2015) Small-Molecule Library Screening by Docking with PyRx. *Chem. Biol.: Method. Protoc*; 243–250. https://doi.org/10.1007/978-1-4939-2269-7_19.
- 44 Cherrak, Y.; Rapisarda, C.; Pellarin, R.; Bouvier, G.; Bardiaux, B.; Allain, F.; Malosse, C.; Rey, M.; Chamot-Rooke, J.; Cascales, E.; Fronzes, R.; Durand, E. (2018) Biogenesis and Structure of a Type VI Secretion Baseplate. *J. Nat. Microbiol.*, 3 (12), 1404–1416. <https://doi.org/10.1038/s41564-018-0260-1>.
- 45 Cui, N.; Zhang, J.-T.; Liu, Y.; Liu, Y.; Liu, X.-Y.; Wang, C.; Huang, H.; Jia, N. (2023) Type IV-A CRISPR-Csf Complex: Assembly, dsDNA Targeting, and CasDinG Recruitment. *J. Mol. Cell*, 83 (14), 2493-2508.e5. <https://doi.org/10.1016/j.molcel.2023.05.036>.
- 46 Chan, P. F.; Srikannathasan, V.; Huang, J.; Cui, H.; Fosberry, A. P.; Gu, M.; Hann, M. M.; Hibbs, M.; Homes, P.; Ingraham, K.; Pizzollo, J.; Shen, C.; Shillings, A. J.; Spitzfaden, C. E.; Tanner, R.; Theobald, A. J.; Stavenger, R. A.; Bax, B. D.; Gwynn, M. N. (2015) Structural Basis of DNA Gyrase Inhibition by Antibacterial QPT-1, Anticancer Drug Etoposide and Moxifloxacin. *J. Nat. Commun.*, 6 (1), 10048. <https://doi.org/10.1038/ncomms10048>.
- 47 Morris, G. M.; Huey, R.; Lindstrom, W.; Sanner, M. F.; Belew, R. K.; Goodsell, D. S.; Olson, A. J. (2009) AutoDock4 and AutoDockTools4: Automated Docking with Selective Receptor Flexibility. *J. Comput. Chem.*, 30 (16), 2785–2791. <https://doi.org/10.1002/jcc.21256>.
- 48 Salah, M.; Belghiti, M.E.; Aitouna, A.O.; Zeroual, A.; Jorio, S.; El Alaoui Abdellaoui, H.; El Hadki, H.; Marakchi, K.; Komiha, N. (2020) MEDT Study of the 1,3-DC Reaction of Diazomethane with Psilostachyin and investigation about the interactions of some pyrazoline derivatives with Protease (Mpro) of nCoV-2. *J. Mol. Graph. Model.*, 107763. <https://doi.org/10.1016/j.jmglm.2020.107763>.
- 49 Morales-Bayuelo, A.; Sanchez-Marquez, J.; Jana, G.; Chattaraj, P. K. (2020) A conceptual DFT analysis of the plausible mechanism of some pericyclic reactions. *Struct. Chem.* <https://doi.org/10.1007/s11224-020-01527-7>.



© 2025 by the authors; licensee Growing Science, Canada. This is an open access article distributed under the terms and conditions of the Creative Commons Attribution (CC-BY) license (<http://creativecommons.org/licenses/by/4.0/>).